

# Model for Transient Enhanced Diffusion of Ion-Implanted Boron, Arsenic, and Phosphorous over Wide Range of Process Conditions

● Kunihiro Suzuki

(Manuscript received January 16, 2003)

We obtained experimental transient enhanced diffusion profiles of boron, arsenic, and phosphorous over a wide range of process conditions. We analyzed these data using a one-dimensional process simulator. By using a simple, empirical methodology for initial super-saturated interstitial Si profiles and a dynamic impurity clustering model, we succeeded in reproducing transient enhanced diffusion profiles with a single parameter set.

## 1. Introduction

Ion implantation for fabricating the source/drain region of MOSFETs generates supersaturated interstitial Si ( $I$ ) and transient enhanced diffusion (TED) is observed in the early stage of the subsequent annealing process.<sup>1)-11)</sup> The junction displacement due to this anomalous diffusion is about 100 nm. The scaling theory requires shallow junctions with decreasing gate length,<sup>12)-15)</sup> and this displacement is critical for designing modern, high-speed MOSFETs.<sup>16)-18)</sup> Therefore, it is important to understand this diffusion phenomenon when designing these devices.

Much work has been done to understand TED, and the following have been identified as the main parameters of this phenomenon:<sup>6)-8)</sup> the time duration of the transient enhanced diffusion  $t_E$ , the enhanced diffusion coefficient during TED  $D_{enh}$ , and the maximum TED concentration  $N_{enh}$ . Empirical models based on empirically derived values of these main parameters have been developed.<sup>8),9)</sup> On the other hand, many attempts have been made to find a theoretical explanation for TED based on the coupled diffusion equation.<sup>19)-22)</sup> Although a consensus for describing TED with basic

transport equations has not been established, some aspects of TED have been clarified. For example, an understanding of the formation of impurity clusters<sup>23)</sup> and the diffusion equation coupled with point defects are indispensable to understanding TED. It is also believed that the interstitial Si is stored in the ion-implanted region in the form of clusters and free interstitial Si is released from these clusters.<sup>24)</sup> While arsenic (As) itself exhibits no significant TED, the ion implantation of As in the source/drain region of a short-channel nMOSFET causes boron (B) TED in the channel region, ultimately leading to reverse short-channel effects.

We obtained experimental B, As, and phosphorous (P) TED data over the wide temperature range of 500 to 1100°C and explained the data using the DIOS process simulator,<sup>21),25)</sup> which considers all of the above-mentioned parameters needed to describe TED.

## 2. Experiment

We ion implanted B, As, and P with various energies and doses into (100) Si substrates under a 7° tilt and 0° rotation. The substrates were then

subjected to furnace annealing (FA) or rapid thermal annealing (RTA) in dry nitrogen. We also investigated TED using epitaxial substrates containing a buried B marker layer to separate the damage effect and the impurity activation mechanism. The loading time was less than 10 s in FA, and the ramp-up rate was 50°C/s in RTA. Substrate heating was performed from both sides of the samples, and the temperature was monitored by a thermocouple.

### 3. Model implemented in DIOS

We will now briefly explain the models implemented in DIOS, simplifying and focusing on the models related to this analysis. Complete explanations of the models are given in Refs. 21) and 25).

#### 3.1 Diffusion equations

The diffusion equations for an impurity, interstitial Si, and vacancy are as follows:<sup>25)</sup>

$$\frac{\partial N}{\partial t} = \frac{\partial}{\partial x} \left\{ \left[ \frac{I}{I^*} f_{\text{ieff}} + \frac{V}{V^*} (1 - f_{\text{ieff}}) \right] \left[ D_{\text{Ai}}^x + \frac{p}{n_i} D_{\text{Ai}}^p + \frac{n}{n_i} D_{\text{Ai}}^m + \left( \frac{n}{n_i} \right)^2 D_{\text{Ai}}^{\text{mm}} \right] \frac{\partial N}{\partial x} \right\} \quad (1)$$

$$\frac{\partial I}{\partial t} = \frac{\partial}{\partial x} \left( D_I \frac{\partial I}{\partial x} \right) - R_{\text{IV}} [IV - I^*V^*] \quad (2)$$

$$\frac{\partial V}{\partial t} = \frac{\partial}{\partial x} \left( D_V \frac{\partial V}{\partial x} \right) - R_{\text{IV}} [IV - I^*V^*] \quad (3)$$

where  $t$  is the time,  $x$  is the depth,  $N$  is the impurity concentration,  $I$  is the interstitial Si concentration,  $V$  is the number of vacancies,  $*$  is the concentration at thermal equilibrium, and  $f_{\text{ieff}}$  is the ratio of diffused impurity pairings to interstitial Si and hence  $(1 - f_{\text{ieff}})$  is the ratio of diffused impurity pairings to vacancies.  $n$  is the electron concentration,  $p$  is the hole concentration, and  $n_i$  is the intrinsic carrier concentration.<sup>26)</sup>  $D_{\text{Ai}}^x$  is the intrinsic diffusion coefficient associated with an impurity pairing with a neutral point defect, and  $D_I$  is the diffusion coefficient associated with a neutral  $I$ .  $D_{\text{Ai}}^p$  is the intrinsic diffusion coefficient

associated with an impurity pairing with a single positive charged point defect,  $D_{\text{Ai}}^m$  is the intrinsic diffusion coefficient associated with an impurity pairing with a single negative charged point defect, and  $D_{\text{Ai}}^{\text{mm}}$  is the intrinsic diffusion coefficient associated with an impurity pairing with a double negative charged point defect.  $D_I$  is the  $I$  diffusion coefficient,  $D_V$  is the  $V$  diffusion coefficient, and  $R_{\text{IV}}$  is the recombination rate of  $I$  and  $V$ .

In thermal equilibrium diffusion,  $I = I^*$ ,  $V = V^*$ , and the profile is simply determined by the following reduced equation:

$$\frac{\partial N}{\partial t} = \frac{\partial}{\partial x} \left\{ \left[ D_{\text{Ai}}^x + \frac{p}{n_i} D_{\text{Ai}}^p + \frac{n}{n_i} D_{\text{Ai}}^m + \left( \frac{n}{n_i} \right)^2 D_{\text{Ai}}^{\text{mm}} \right] \frac{\partial N}{\partial x} \right\} \quad (4)$$

In the intrinsic semiconductor, where the doping concentration is less than  $n$ ,  $p = n = n_i$  and Eq. 4 reduces to:

$$\frac{\partial N}{\partial t} = D_{\text{Ai}} \frac{\partial^2 N}{\partial x^2} \quad (5)$$

where

$$D_{\text{Ai}} = D_{\text{Ai}}^x + D_{\text{Ai}}^p + D_{\text{Ai}}^m + D_{\text{Ai}}^{\text{mm}} \quad (6)$$

#### 3.2 Initial condition for supersaturated interstitial Si concentration profile

The supersaturated  $I$  is introduced by ion implantation. The empirical expression of  $I$  distribution was proposed by Giles<sup>27)</sup> and is called the +1 model. The initial  $I$  profile  $I(x,0)$  is the same as the ion implanted profile, which is given by:

$$I(x, 0) = 1 \times \Phi g(x) \quad (7)$$

where  $g(x)$  is the ion implanted impurity concentration normalized by the dose  $\Phi$ . However, this treatment is too simple to cover various conditions. We therefore propose the following methodology for generating  $I(x, 0)$ .

We assume that each ion implanted impurity generates the same amount of  $I$  at low doses and that all impurities identically contribute to the generation of  $I$ . Once the damage level has reached a certain value,  $I$  cannot be generated

any more. Therefore, we propose that the initial  $I$  is expressed by:

$$I(x, 0) = \begin{cases} f_D \Phi g(x) & \text{for } \Phi < \Phi_c \\ f_D \Phi_c g(x) & \text{for } \Phi > \Phi_c \end{cases} \quad (8)$$

where the damage factor  $f_D$  has a fixed value independent of the dose  $\Phi$ .  $\Phi_c$  is the critical dose for TED saturation, and doses exceeding  $\Phi_c$  do not contribute to the generation of  $I$ .

### 3.3 Interstitial Si clustering model

The generated supersaturated  $I$  are believed not to diffuse simply, but to form (311) defects.<sup>28)</sup> These defects become large and then release mobile  $I$ . The dynamic treatment is complex, but we empirically express the features using the solid solubility of  $I$  as  $I_{sol}$ . These parameters should be used for all impurity diffusions.

### 3.4 Impurity clustering model and solid solubility

The following non-equilibrium impurity cluster model was proposed in Ref. 29), which leads to the time evolution of the impurity cluster:

$$m \frac{\partial N_m}{\partial t} = k_f \frac{1}{N^{d_c}} \left( \frac{n}{n_i} \right)^{k_c} \left[ N^m - \frac{N_m}{N_0} \left( \frac{N_{sol}}{n_i} \right)^m N_{sol}^m \left( \frac{n}{n_i} \right)^m \right] \quad (9)$$

where  $N_0$  is the cluster concentration where  $N$  reaches its solubility  $N_{sol}$ ,  $N_m$  is the cluster concentration, and  $m$  is the number of impurities in one cluster.  $d_c$  and  $k_c$  are parameters associated with the chemical reaction of cluster formation and are fitting parameters since the reaction is not well established. The left side of Eq. (9) is the time evolution of the impurity concentration that forms clusters and has the factor  $m$ , since one cluster contains  $m$  impurities.

## 4. Results and discussion

The value of the thermal equilibrium diffusion coefficient has been rather well established by various reports.<sup>30)</sup> However, the values given in these reports were extracted at temperatures higher than 900°C. Therefore, we evaluated the thermal equilibrium diffusion coefficient over a wide temperature range with a low dose and a high thermal budget. We then analyzed the TED parameters with a high dose and a low thermal budget.

### 4.1 Thermal equilibrium diffusion

Figures 1 to 3 show the diffusion profiles of B, As, and P, respectively. The ion implantation dose is low, and the thermal budget is quite high

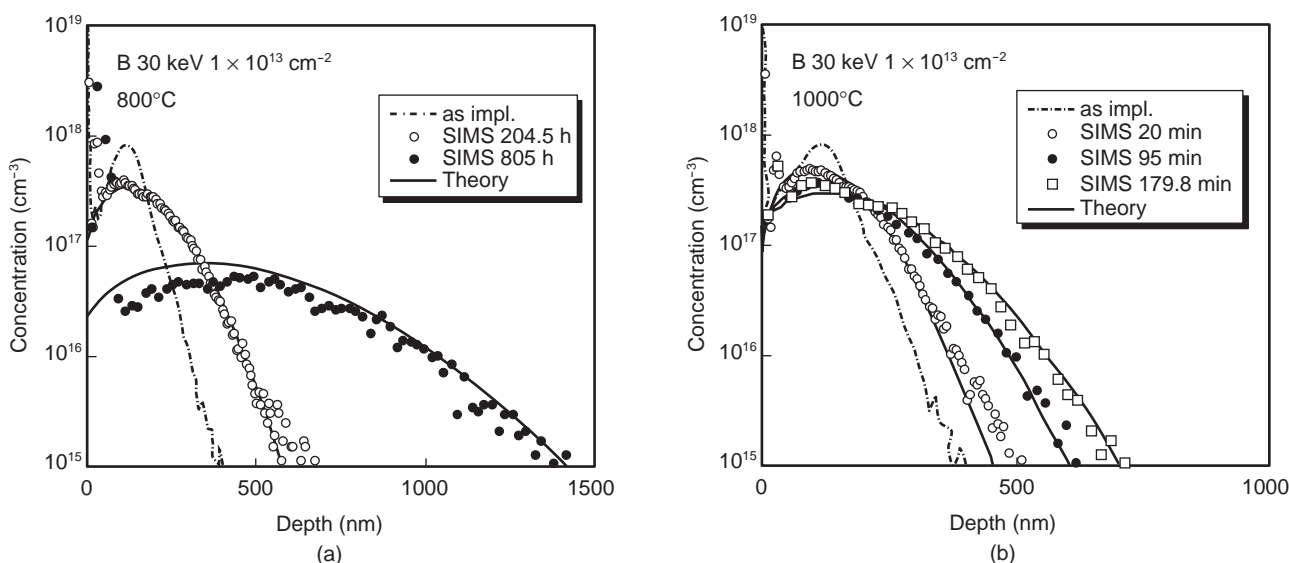


Figure 1 Thermal equilibrium diffusion profiles of B. (a) 800°C. (b) 1000°C.

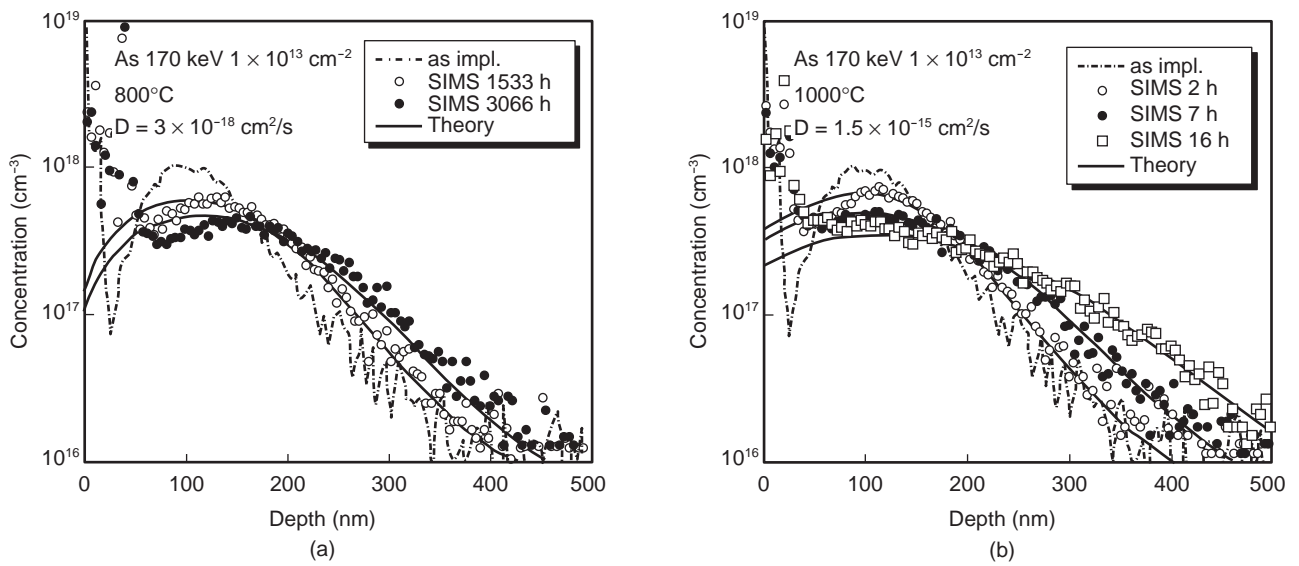


Figure 2  
Thermal equilibrium diffusion profiles of As. (a) 800°C. (b) 1000°C.

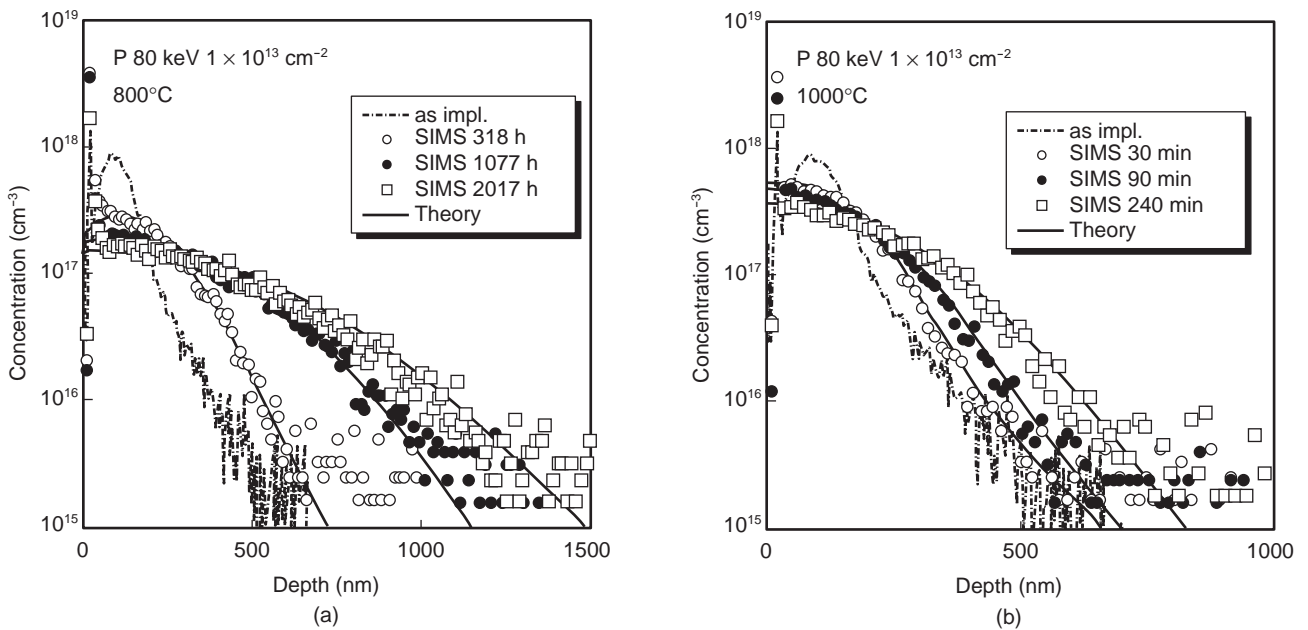


Figure 3  
Thermal equilibrium diffusion profiles of P. (a) 800°C. (b) 1000°C.

to eliminate the TED effects.

We fitted the diffusion profiles of B, As, and P. The extracted diffusion coefficients are shown in **Figures 4 to 6**. These values agree well with

reported values at high temperatures exceeding 900°C. However, the value is not expressed by a single activation energy at low temperatures. All these data are well expressed by:

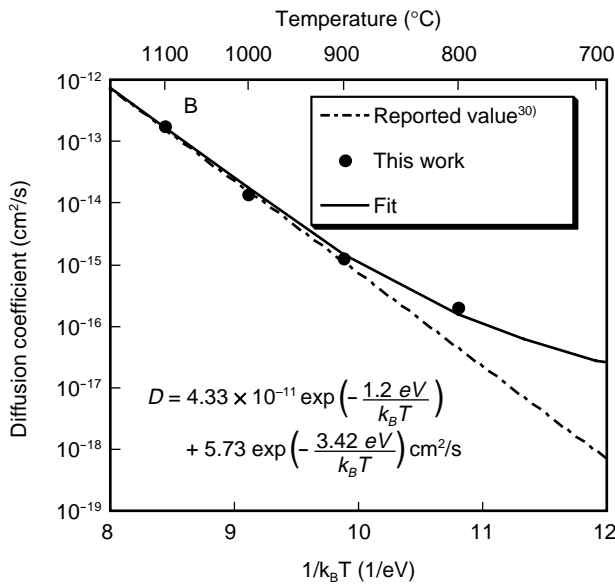


Figure 4  
Diffusion coefficient of B.

$$D(B) = 4.33 \times 10^{-11} \exp\left(-\frac{1.2 \text{ eV}}{k_B T}\right) + \left(\frac{p}{n_i}\right) 5.73 \exp\left(-\frac{3.42 \text{ eV}}{k_B T}\right) \text{ cm}^2/\text{s} \quad (10)$$

$$D(\text{As}) = 5.00 \times 10^{-9} \exp\left(-\frac{2.00 \text{ eV}}{k_B T}\right) + \left(\frac{n}{n_i}\right) 5.12 \exp\left(-\frac{3.93 \text{ eV}}{k_B T}\right) \text{ cm}^2/\text{s} \quad (11)$$

$$D(\text{P}) = 1.40 \times 10^{-7} \exp\left(-\frac{2.00 \text{ eV}}{k_B T}\right) + \left(\frac{n}{n_i}\right) 5.77 \exp\left(-\frac{3.67 \text{ eV}}{k_B T}\right) \text{ cm}^2/\text{s} \quad (12)$$

where  $n = p = n_i$  in the experiments associated with Figures 1 to 3. We assume that the diffusion coefficient in the high concentration region corresponds to the diffusivity associated with charged point defects. The separation of the total diffusivity into the individual components should be investigated.

## 4.2 Transient enhanced diffusion

### 4.2.1 B

We succeeded in explaining the data of the B

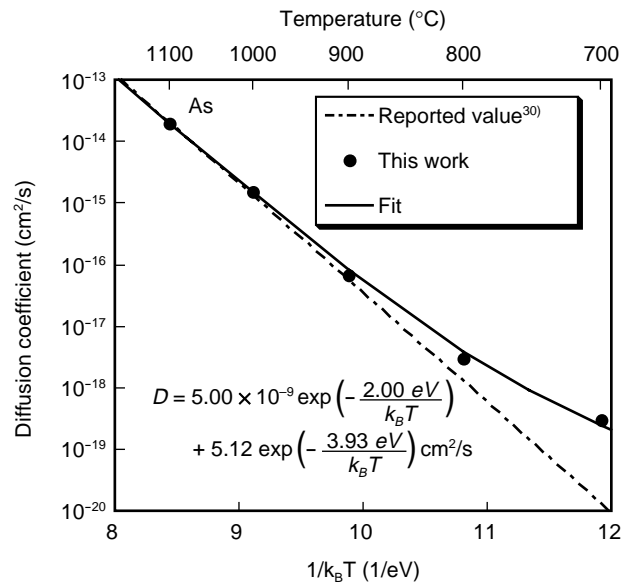


Figure 5  
Diffusion coefficient of As.

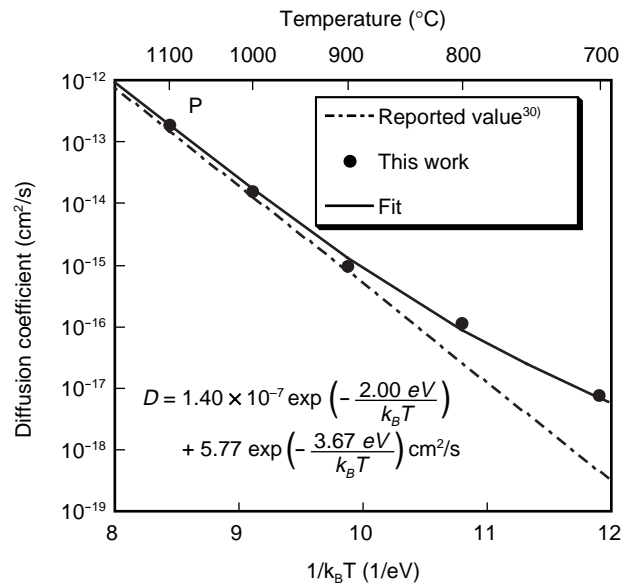


Figure 6  
Diffusion coefficient of P.

TED profiles as shown in **Figures 7 to 9**. We used the B solid solubility  $N_{sol}$  and the I solubility  $I_{sol}$  as fitting parameters. Their values are shown in **Figure 10**.  $f_D$  was 2, and  $\Phi_c$  was  $1 \times 10^{14} \text{ cm}^{-2}$ .  $f_{ieff}$  is 0.94, and the parameters associated with the clustering model are summarized in **Table 1**.

TED displacement is enhanced at low tem-

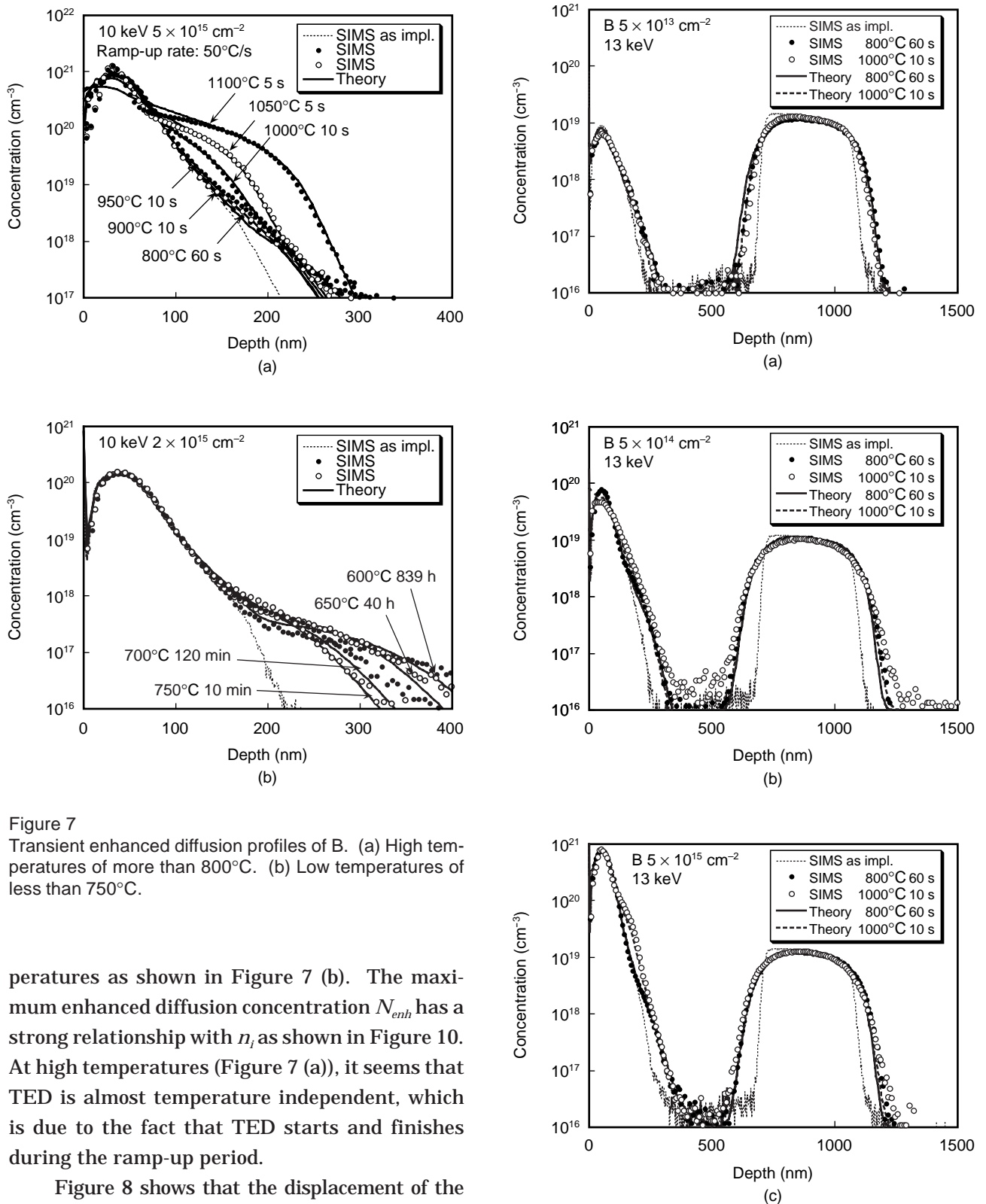


Figure 7  
Transient enhanced diffusion profiles of B. (a) High temperatures of more than  $800^\circ\text{C}$ . (b) Low temperatures of less than  $750^\circ\text{C}$ .

peratures as shown in Figure 7 (b). The maximum enhanced diffusion concentration  $N_{enh}$  has a strong relationship with  $n_i$  as shown in Figure 10. At high temperatures (Figure 7 (a)), it seems that TED is almost temperature independent, which is due to the fact that TED starts and finishes during the ramp-up period.

Figure 8 shows that the displacement of the buried B layer is insensitive to the dose at  $800^\circ\text{C}$  for 60 s. On the other hand, the displacement is significantly suppressed at a dose of  $5 \times 10^{13} \text{ cm}^{-2}$  at  $1000^\circ\text{C}$  for 10 s. The theory expresses the phenomenon

Figure 8  
Dependence of transient enhanced diffusion profiles of B with buried B marker layer on dose. (a)  $5 \times 10^{13} \text{ cm}^{-2}$ . (b)  $5 \times 10^{14} \text{ cm}^{-2}$ . (c)  $5 \times 10^{15} \text{ cm}^{-2}$ .

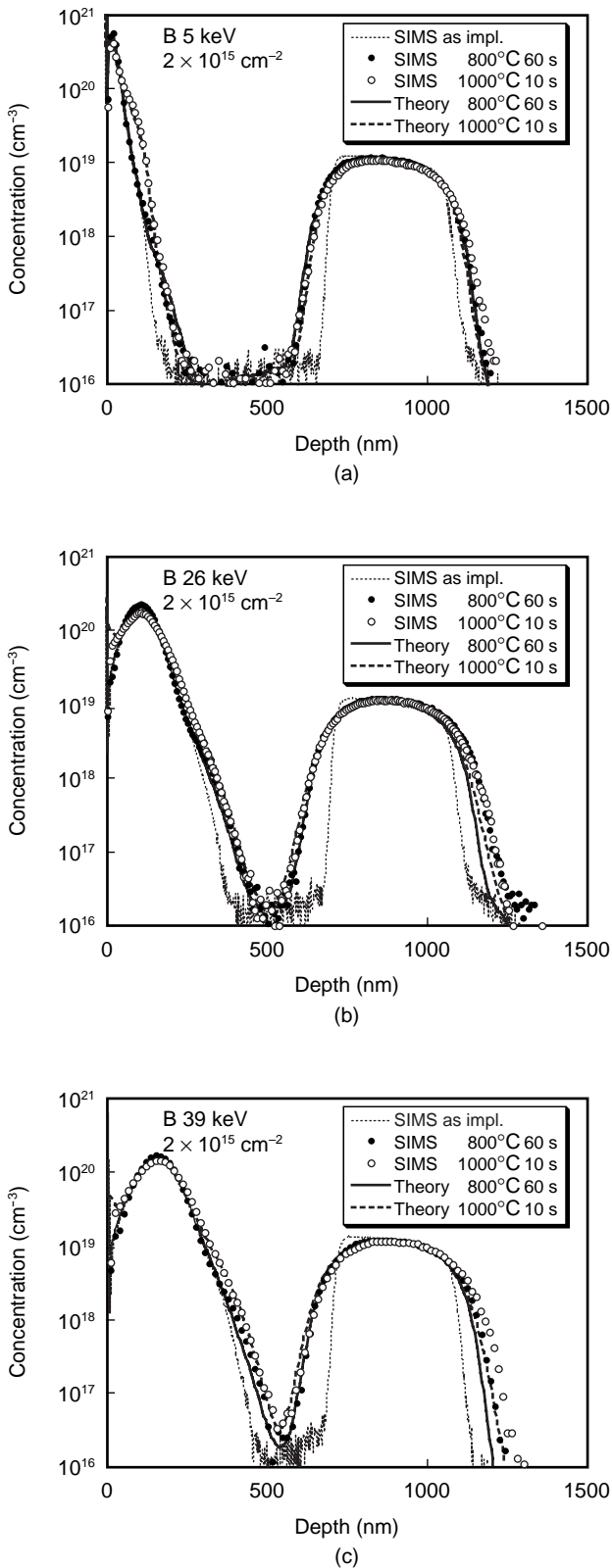


Figure 9  
Dependence of transient enhanced diffusion profiles of B with buried B marker layer on energy. (a) 5 keV. (b) 26 keV. (c) 39 keV.

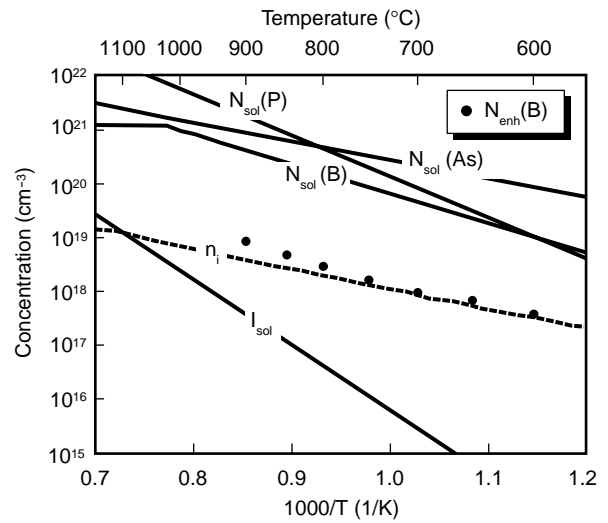


Figure 10  
Dependence of solid solubility, intrinsic carrier concentration, and maximum B transient enhanced diffusion concentration on temperature.

Table 1  
Parameters associated with impurity clustering.

	dc	kc	m
B	1	-1	3
As	0	3	3
P	1	-1	3

quantitatively and explains this as follows.

**Figure 11** shows the calculated time dependence of the buried-layer impurity displacement  $L_D$  using the parameter values that we extracted.  $L_D$  is defined by the displacement where the concentration  $N_j$  reaches  $10^{17} \text{ cm}^{-3}$  as shown in the inset in Figure 11. We assumed an isothermal process to clarify the phenomenon related to the temperature. If TED is in progress, which is the case in the  $800^\circ\text{C}$  60 s experiment, a constant  $I$  concentration is supplied continuously and  $L_D$  only depends on the time and is independent of the total amount of  $I$  (i.e., the dose).

When the dose is  $5 \times 10^{15} \text{ cm}^{-2}$ ,  $L_D$  at  $900^\circ\text{C}$  for 10 s coincides with  $L_D$  at  $800^\circ\text{C}$  for 60 s. Also, when the dose is  $5 \times 10^{15} \text{ cm}^{-2}$ ,  $L_D$  at  $1000^\circ\text{C}$  for 10 s is much shorter than  $L_D$  at  $800^\circ\text{C}$  for 60 s. This means

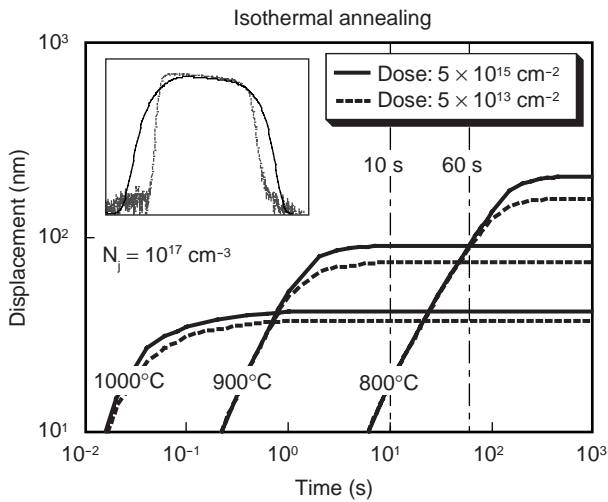


Figure 11 Dependence of diffusion length on annealing time with various temperatures. The ramp-up period is ignored.

that  $L_D$  at 1000°C is determined during the ramp-up period instead of during the isothermal process at 1000°C. Therefore,  $L_D$  at 1000°C is effectively determined at 900°C during the ramp-up period.

If the annealing time is longer than the TED duration, which should be the case at 1000°C for 10 s in the experiment, then  $L_D$  depends on the total amount of  $I$ . This is the reason why  $L_D$  is suppressed at  $5 \times 10^{13} \text{ cm}^{-2}$  at 1000°C.

The above explanation is also valid for the results shown in Figure 7 (a); that is, the TED profile is determined during the ramp-up period for temperatures exceeding 900°C and the TED profiles at these temperatures are the same. By chance, as shown in Figure 11, the TED profiles at 800°C for 60 s coincide with the profiles at the other temperatures.

The selective low-concentration diffusion is as follows:

TED occurs in the early stage of diffusion, and the B are not fully activated to  $N_{\text{sol}}$ . Therefore, a dynamic activation model such as Eq. (9) is indispensable.

The dependence of TED on the energy is also well simulated as shown in Figure 9. TED is suppressed as the energy is decreased.  $I$  are

dominantly consumed at the surface, and the low implant energy leads to a fast consumption of  $I$ , resulting in suppressed TED.

#### 4.2.2 As

Figure 12 shows the As dose dependence of diffusion profiles. While the As diffusion is quite small as was expected, the TED of buried-layer B is significant. For a damage  $f_D = 2$  and a critical dose of  $1.5 \times 10^{14} \text{ cm}^{-2}$ , excellent agreement is obtained between SIMS results and the simulated profiles. The solid solubilities are shown in Figure 10, and the parameters associated with clustering are summarized in Table 1.

For the 1000°C, 10 s anneal, the displacement of the buried-layer B increases with an increase in dose from  $5 \times 10^{13}$  to  $5 \times 10^{14} \text{ cm}^{-2}$  and then saturates. In our model, we can explain this result through the dependence of the effective dose.

For the 800°C, 60 s anneal, the displacement of the buried B layer is insensitive to the As dose. With these annealing conditions, TED only begins to occur and is not fully expressed. During the TED time period, a constant  $I$  concentration is supplied continuously from  $I$  clusters and the displacement depends only on the time and not on the total amount of  $I$  (i.e., the dose).

Although the TED of As is not significant, the redistribution was observed as shown in Figure 13. We tuned  $f_{\text{eff}}$  to express the insignificant TED of As and succeeded in explaining the redistribution of As at the surface region with an  $f_{\text{eff}}$  of 0.03. This means that the contribution of the As- $I$  pair diffusion to the total As diffusion is quite small.

#### 4.2.3 P

Figure 14 shows the P dose dependencies of diffusion profiles.

The solid solubility is shown in Figure 10, and the parameters associated with clusters are shown in Table 1.  $f_D$  was 1.8, and  $\Phi_c$  was  $1.34 \times 10^{14} \text{ cm}^{-2}$ .

At the low dose of  $5 \times 10^{13} \text{ cm}^{-2}$ , the displacements of P and B concentration profiles are larger

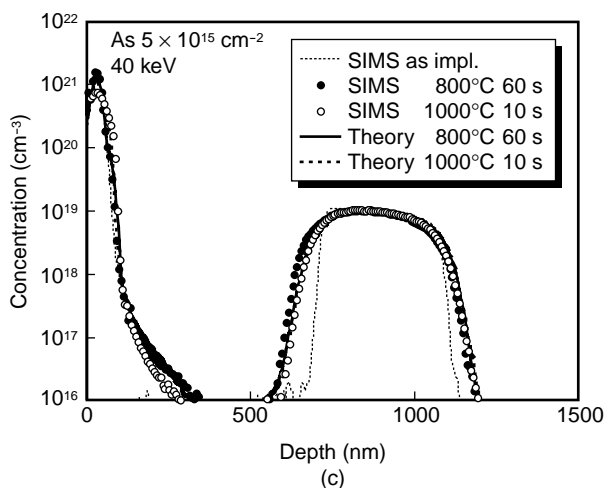
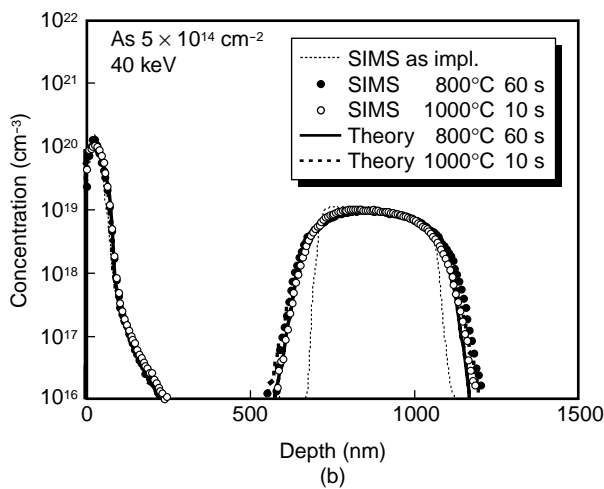
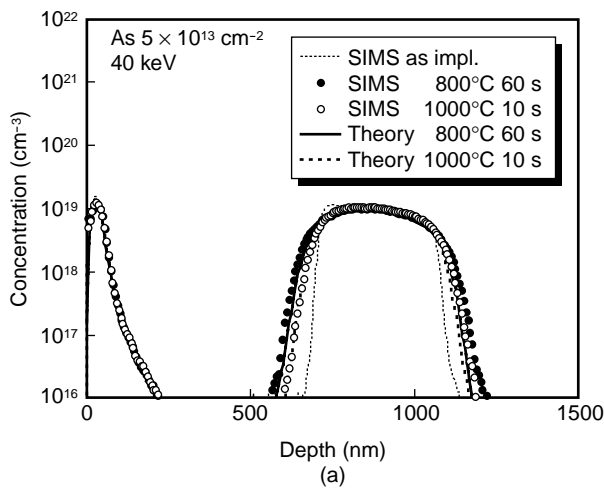


Figure 12  
Dependence of transient enhanced diffusion profiles of As with buried B marker layer on dose. (a)  $5 \times 10^{13} \text{ cm}^{-2}$ . (b)  $5 \times 10^{14} \text{ cm}^{-2}$ . (c)  $5 \times 10^{15} \text{ cm}^{-2}$ .

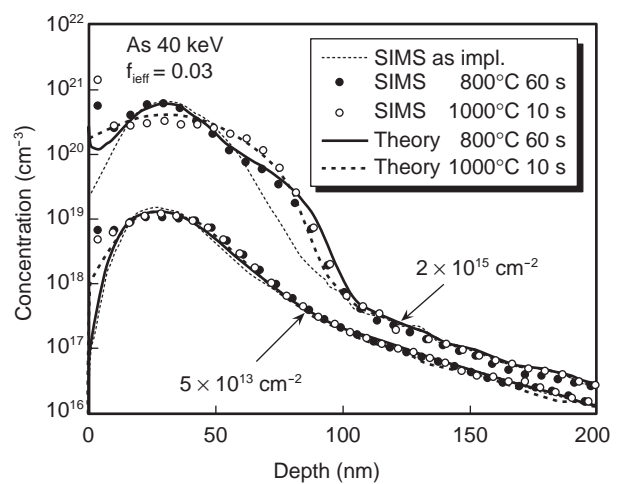


Figure 13  
Dependence of surface diffusion profiles of As.

at 800°C than at 1000°C (Figure 14 (a)), which is a prominent feature of TED. When the dose is increased, the displacement increases and then saturates and both the buried-layer B profiles and the P profiles in the low-concentration region are also insensitive to temperature. P TED selectively occurs in the low-concentration region at 800°C annealing, which is similar to the case of ion-implanted B diffusion profiles.

For the 1000°C, 10 s anneal, the displacement of the buried-layer B increases with an increase in dose from  $5 \times 10^{13}$  to  $5 \times 10^{14} \text{ cm}^{-2}$  and then saturates. In our model, we can explain this result through the dependence of the effective dose.

For the 800°C, 60 s anneal, the displacement of the buried B layer is insensitive to the P dose. With these annealing conditions, TED only begins to occur and is not fully expressed. During the TED time period, a constant  $I$  concentration is supplied continuously from  $I$  clusters and the displacement depends only on the time and not on the total amount of  $I$  (i.e., the dose).

It is noteworthy that, as summarized in **Table 2**, the extracted  $f_D$  and  $\Phi_c$  are almost insensitive to impurities since the induced damage features should be quite different between impurities. When there is high-density  $I$  generation,

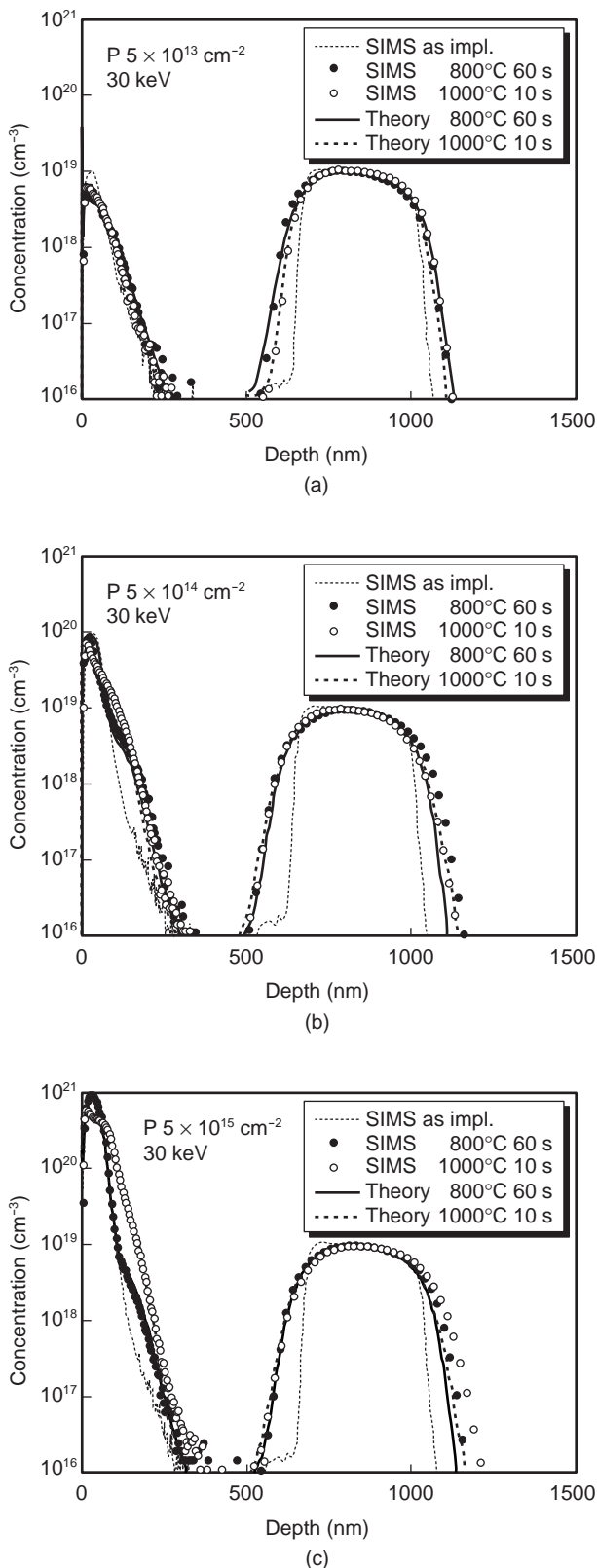


Figure 14  
Dependence of transient enhanced diffusion profiles of P with buried B marker layer on dose. (a)  $5 \times 10^{13} \text{ cm}^{-2}$ . (b)  $5 \times 10^{14} \text{ cm}^{-2}$ . (c)  $5 \times 10^{15} \text{ cm}^{-2}$ .

Table 2

Parameters associated with supersaturated interstitial Si due to ion implantation.

	$f_D$	$\Phi_c \text{ (cm}^{-2}\text{)}$
B	2	1.13E+14
As	2	1.50E+14
P	1.8	1.34E+14

it must also be accompanied by high-density vacancy  $V$  generation and a significant recombination of  $I$  and  $V$  should occur. Our model considers only supersaturated  $I$  and not  $V$ , and hence the generated  $I$  in our model correspond to the residual  $I$  after this recombination process. The similar values of  $f_D$  for all three impurities in Table 2 suggests that the residual  $I$ , which are believed to contribute to the TED of impurities, are insensitive to the ion implanted impurities.

## 5. Summary

We demonstrated that our methodology for generating interstitial Si ( $I$ ) can explain all redistribution profiles of B, As, and P with a single parameter set. We showed that the parameters associated with our methodology for generating  $I$  are insensitive to impurities. A dynamic clustering model for impurities is indispensable for selectively expressing the TED in diffusion profiles that are lower than the solid solubility.

## Acknowledgement

The author wishes to thank Dr. A. Hoefler, Dr. T. Feudel, Dr. N. Strecker, and Dr. W. Fichtner for their invaluable discussions; Mr. Y. Kataoka for the SIMS measurements; and Dr. N. Sasaki for his encouragement.

## References

- 1) P. M. Fahey, J. L. Newton, and J. D. Plummer: Points defects and dopant diffusion in silicon. *Rev. Mod. Phys.*, **61**, p.289-384 (1984).
- 2) A. E. Michel, W. Rausch, P. A. Ronsheim, and R. H. Kastl: Rapid annealing and the anomalous diffusion of ion implanted boron into

- silicon. *Appl. Phys. Lett.*, **50**, p.416-418 (1987).
- 3) A. E. Michel, W. Rausch, and P. A. Ronsheim: Implantation damage and the anomalous transient diffusion of ion-implanted boron. *Appl. Phys. Lett.*, **51**, p.4487-4489 (1987).
  - 4) T. O. Sedwick, A. E. Michel, V. R. Deline, and S. A. Cohen: Transient boron diffusion in ion implanted crystalline and amorphous silicon. *J. Appl. Phys.*, **63**, p.1452-1463 (1988).
  - 5) M. D. Giles: Defect-coupled diffusion at high concentrations. *IEEE Trans. Computer-Aided Design*, **8**, p.460-467 (1989).
  - 6) R. B. Fair: Points defect charge-state effects on transient diffusion of dopants in Si. *J. Electrochem. Soc.*, **137**, p.667-671 (1990).
  - 7) N. E. B. Cowern, K. T. F. Janssen, and H. F. F. Jos: Transient diffusion of ion-implanted B in Si: Dose, time and matrix dependence of atomic and electrical profiles. *J. Appl. Phys.*, **68**, p.6191-6198 (1990).
  - 8) S. Solmi, F. Baruffaldi, and R. Canteri: Diffusion of boron in silicon during post-implantation annealing. *J. Appl. Phys.*, **69**, p.2135-2142 (1991).
  - 9) H. R. Soleimani: Modeling of high-dose ion implantation-induced dopant transient diffusion, and dopant transient activation in silicon (boron and arsenic diffusion). *J. Electrochem. Soc.*, **139**, p.3275-3284 (1992).
  - 10) A. J. Walker, P. H. Woerree, H. G. Pomp, and N. E. B. Cowern: Shallow boron junctions and preamorphization for deep submicron silicon technology. *J. Appl. Phys.*, **73**, p.4048-4053 (1993).
  - 11) P. A. Stolk, H.-J. Gossmann, D. J. Eaglesham, D. C. Jacobson, and J. M. Poate: Trap-limited interstitial diffusion and enhanced boron clustering in silicon. *Appl. Phys. Lett.*, **66**, p.568-570 (1995).
  - 12) R. H. Dennard, F. H. Gaensslen, H. N. Yu, V. L. Rideout, E. Bassous, and A. L. Blanc: Design of ion-implanted MOSFETs with very small physical dimensions. *IEEE J. Solid-State Circuits*, **9**, p.256-268 (1974).
  - 13) J. R. Brews, W. Fichtner, E. H. Nicollian, and S. M. Sze: Generalized guide for MOSFET miniaturization. *IEEE Electron Dev. Lett.*, **1**, p.2-4 (1980).
  - 14) P. Chatterjee, W. R. Hunter, T. C. Holloway, and Y. T. Lin: The impact of scaling laws on the choice of n-channel or p-channel for MOS VLSI. *IEEE Electron Dev. Lett.*, **1**, p.220-223 (1980).
  - 15) G. Baccarani, M. R. Wordeman, and R. H. Dennard: Generalized scaling theory and its application to a 1/4 micrometer MOSFET design. *IEEE Trans. Electron Dev.*, **31**, p.452-462 (1984).
  - 16) G. G. Shahidi, J. Warnock, A. Acovic, P. A. Agnello, C. Blair, T. Bucelot, A. Burghartz, J. Cressler, P. Coane, J. Comfort, B. Davari, S. Fischer, E. Ganin, S. Gittleman, J. Keller, K. Jenkins, D. Klaus, K. Keiwtniak, T. Lii, P. A. McFarland, T. Ning, M. Polcari, S. Subbana, J. Y. Sun, D. Sunderland, A. C. Warren, and C. Wong: A high performance 0.15  $\mu\text{m}$  CMOS. Symp. VLSI Tech., p.93-94, 1993.
  - 17) K. F. Lee, R. H. Yan, D. Y. Jeon, G. M. Chin, Y. O. Kim, D. M. Tennant, B. Razavi, H. D. Lin, Y. G. Wey, E. H. Westerwick, M. D. Morris, R. W. Jhonson, T. M. Liu, M. Cerullo, R. G. Swartz, and A. Ourmazd: Room temperature 0.1  $\mu\text{m}$  CMOS technology with 11.8 ps gate delay. IEDM Tech. Dig., p.131-134, 1993.
  - 18) M. Iwase, T. Mizuno, M. Takahashi, H. Nijiyama, M. Fukumoto, K. Ishida, S. Inaba, Y. Takigami, A. Sanada, A. Toriumi, and M. Yoshimi: High-performance 0.10- $\mu\text{m}$  CMOS devices operating at room temperature. *IEEE Electron Dev. Lett.*, **14**, p.51-53 (1993).
  - 19) M. E. Law: Parameters for point-defect diffusion and recombination. *IEEE Trans. Computer-Aided Design*, **7**, p.1125-1131 (1991).
  - 20) M. Hane and H. Matsumoto: A model for bo-

- ron short time annealing after ion implantation. *IEEE Trans. Electron Dev.*, **40**, p.1215-1222 (1993).
- 21) A. Hoefler, T. Feudel, N. Strecker, and W. Fichtner: A technology oriented model for transient diffusion and activation in silicon. *J. Appl. Phys.*, **78**, p.3671-3679 (1995).
- 22) B. Baccus and E. Vandenbossche: A continuous and general model for boron diffusion during post implant annealing including damaged and amorphizing conditions. *IEEE Trans. Semicon. Manufa.*, **9**, p.59-66 (1996).
- 23) D. Mathiot and J. C. Pfister: Dopant diffusion in silicon: A consistent view involving nonequilibrium defects. *J. Appl. Phys.*, **55**, p.3518-3530 (1984).
- 24) D. J. Eaglesham, P. A. Stolk, H.-J. Gossmann, and J. M. Poate: Implantation and transient diffusion in Si: The source of the interstitial. *Appl. Phys. Lett.*, **65**, p.2305-2307 (1994).
- 25) A. Hoefler and N. Strecker: On the coupled diffusion of dopants and silicon point defects. ETH technical report 94/11.
- 26) F. J. Morrin and J. P. Maita: Electrical properties of silicon containing arsenic and boron. *Phys. Rev.*, **96**, p.28-35 (1954).
- 27) M. D. Giles; Transient phosphorous diffusion below the amorphization threshold. *Appl. Phys. Lett.* **62**, p.1940-1942 (1993).
- 28) P. A. Stolk, H. J. Gossmann, D. J. Eaglesham, D. C. Jacobson, C. S. Rafferty, G. H. Gilmer, M. Jaraiz, and J. M. Poate: Physical mechanisms of transient enhanced dopant diffusion in ion-implanted silicon. *J. Appl. Phys.*, **81**, p.6031-6050 (1997).
- 29) A. Hoefler, T. Feudel, A. Liegmann, N. Strecker, W. Fichtner, K. Suzuki, and N. Sasaki: Precipitation phenomena and transient diffusion/activation during high concentration boron annealing. SISDEP, p.448-451, 1995.
- 30) S. M. Sze: VLSI Technology. McGraw-Hill, New York, 1988.



**Kunihiro Suzuki** received the B.S., M.S., and Ph.D. degrees in Electronics Engineering from Tokyo Institute of Technology, Tokyo, Japan in 1981, 1983, and 1996, respectively. He joined Fujitsu Laboratories Ltd., Atsugi, Japan in 1983, where he has been engaged in design and modeling of high-speed bipolar and MOS transistors. He was a visiting researcher at the Swiss Federal Institute of Technology (ETH) Zurich,

Switzerland in 1996 and 1997, where he studied process modeling. His current interests are process and device modeling. He is a senior member of the IEEE.

E-mail: [suzuki.kunihiro@jp.fujitsu.com](mailto:suzuki.kunihiro@jp.fujitsu.com)